npj | clean water

Article

Published in partnership with King Fahd University of Petroleum & Minerals

https://doi.org/10.1038/s41545-024-00362-1

Tuning polyamide membrane chemistry for enhanced desalination using Boc-protected ethylenediamine and its in situ Boc-deprotection

Hilal Ahmad[1], Abdul Waheed[1] ✉, Fahad Ayesh Alharthi[2], Christopher Michael Fellows[2,3], Umair Baig[1] & Isam H. Aljundi[1,4] ✉

The scarcity of freshwater resources, driven by rapid population growth and industrialization, underscores the urgent need for advanced desalination technologies. This research aims to meet this critical demand by enhancing the performance of polyamide membranes through innovative chemical tuning of the active layer. By strategically using Boc-protected ethylenediamine (EDA), we can precisely control the membrane's surface properties. One amino group in EDA is protected with a Boc group, allowing the other to participate in the interfacial polymerization (IP) reaction with meta-phenylenediamine (MPD) and trimesoyl chloride (TMC). This inclusion of Boc-protected EDA enables in situ tuning of the active layer chemistry during polymerization. Subsequent removal of the Boc protection generates hydrophilic ammonium groups on the membrane surface, enhancing its desalination capabilities. As a result, three distinct membranes were fabricated and thoroughly characterized: MPD-TMC (control), MPD-TMC-EDA-Boc, and MPD-TMC-EDA-Deboc. At 20 bar and 2000 ppm NaCl feed, the MPD-TMC-EDA-Deboc membrane demonstrated superior desalination performance with a salt rejection of 98 ± 0.5% and a permeate flux of 25 L m^{-2} h^{-1}; an increase of 25% compared to the control membrane. For the seawater nanofiltration (NF) permeate with a TDS of 33,700 ppm, a salt rejection of 97% and a permeate flux of 23 L m^{-2} h^{-1} was recorded at 20 bar. The MPD-TMC-EDA-Deboc membrane showed enhanced antifouling performance (95 ± 1% flux recovery) compared to the control MPD-TMC membrane with 93 ± 1% flux recovery. The Boc-protection/deprotection strategy demonstrated the high potential of this approach to significantly enhance the performance of polyamide membranes for desalination applications.

The discovery of polyamide membranes four decades ago revolutionized the whole desalination industry worldwide[1]. Since then, polyamide membranes prepared by interfacial polymerization (IP) have served humanity by providing clean and drinkable water. The development of reverse osmosis (RO) membranes with a fully aromatic polyamide network (typically m-phenylenediamine-trimesoyl chloride (MPD/TMC)) as an active layer has largely replaced the cellulose-based integrally skinned asymmetric (IAS) membranes developed by Loeb and Sourirajan[2]. Compared to IAS membranes, polyamide thin film composite (TFC) membranes are prepared by IP which provides a composite structure where one thin film is deposited on another film[3,4]. Compared to IAS membrane fabrication, IP offers more freedom of controlling the chemistry and structure of each layer separately leading to a membrane with optimized performance in terms of flux and salt rejection. Owing to their exceptional performance, easy and facile scaling-up at an industrial scale, these membranes now dominate the industrial desalination market[5]. Recently, a new concept of developing semi-

[1]Interdisciplinary Research Center for Membranes and Water Security, King Fahd University of Petroleum & Minerals (KFUPM), Dhahran, Saudi Arabia. [2]Water Technologies Innovation Institute & Research Advancement (WTIIRA), Saline Water Conversion Corporation (SWCC), PO Box 8284 Al-Jubail, Kingdom of Saudi Arabia. [3]School of Science and Technology, The University of New England, Armidale, NSW, Australia. [4]Chemical Engineering Department, King Fahd University of Petroleum & Minerals (KFUPM), Dhahran, Saudi Arabia. ✉e-mail: abdul.waheed@kfupm.edu.sa; aljundi@kfupm.edu.sa

aromatic membranes has been put forward for tuning the chemistry, structure, and performance of the membranes[6]. Semi-aromatic polyamide membranes have been developed by IP reactions between amines and acid chlorides such as the IP between piperazine (PIP) and TMC is a well-known example of preparing semi-aromatic NF membranes[7]. These developments are attributed to the versatile IP process which is not limited only to polyamide synthesis but has also found widespread applications including the synthesis of polyureas, polyurethanes, polyesters, polycarbonates, and polysulfonamides[8]. This success of the IP process in developing remarkably thin selective films is attributed to features such as (i) the self-limiting kinetics where the IP process slows down with the progression of time and hence the growth of the thin film is stopped automatically[9]; (ii) self-sealing potential attributed the ability of the IP process to direct the reaction to the more permeable sites which results in sealing the potential pores of the polyamide active layer; and (iii) crosslinking of the growing polyamide chains due to the use of a trifunctional monomer such as TMC[10]. Hence, there lies a huge potential in tuning the chemistry of the membrane's active layers by using the IP approach.

Despite all the promising features of the polyamide membranes developed by IP, there are still several challenges that provide scope for further research. The major challenges include trade-offs between permeate flux and salt rejection, chlorine resistance, antifouling properties, life span, and anti-biofouling potential of the polyamide membranes. Two main strategies have been adopted by researchers to enhance the performance of polyamide desalination membranes. The first strategy is to synthesize new active layers using new reactive monomers during IP whereas the second strategy is modifying the active layer of the membrane by chemical or physical methods.

Adopting the first strategy is somewhat challenging owing to the expertise required for synthesizing new molecules for IP and hence has not been widely explored in literature for fabricating new desalination membranes. The second strategy is easy to carry out and hence most of the literature has been dedicated to tuning the membrane structure by adding new chemical additives to enhance the performance of the desalination membranes[11–14]. In a work carried out by Yong et al.[15], m-phenylenediamine-5-sulfonic acid was added after polymerization to enhance the desalination features of aromatic polyamide membranes. At an optimized concentration of m-phenylenediamine-5-sulfonic acid, a 1.4 times enhancement in permeate flux was achieved with NaCl rejection nearly like that of the control MPD-TMC membrane. This increase in permeate flux was attributed to the presence of hydrophilic sulfonic acid groups in the active layer of the membrane. Similarly, in another work carried out by Prera et al.[16], an effort was made to regulate the aqueous phase composition of the MPD/TMC membrane where a linear aliphatic amine 1,3-diamino-2-hydroxypropane (DAHP) was added to the aqueous phase. The resultant membrane showed an improvement of 22% in permeate flux while keeping the salt rejection (96 -98%) nearly the same as that of the MPD/TMC control membrane.

Several aliphatic basic amino acids have also been explored as a potential route to enhance the performance of the desalination membranes. For instance, Chen et al. used $_{L}$-arginine (Arg) as an aqueous additive along with MPD monomer during IP with TMC leading to an RO membrane which resulted in the enhancement of both permeate flux and salt rejection. With 0.5% content of Arg in the MPD solution, the resultant membrane showed an improvement in permeate flux from 46 ± 0.5 L m^{-2} h^{-1} to 54 ± 0.5 L m^{-2} h^{-1} whereas the rejection of salt was increased from $96 \pm 0.5\%$ to $98 \pm 0.5\%$[17]. The existence of aliphatic flexible linear chains along with some functionalities such as carboxylic groups, amino groups, and sulfonic acid groups in the backbone of the polyamide active layer results in increasing the permeate flux of the membranes while keeping the rejection rate of salts considerably higher. In a work carried out by Xu et al., a linear aliphatic basic amino acid $_{L}$-lysine was used as an aqueous additive in the MPD solution. Upon IP reaction with TMC, the resultant membrane demonstrated an 18% enhancement in the permeate flux whereas the salt rejection remained unaffected[18]. Hence, there lies a huge potential in tuning the performance of the desalination membranes by regulating the aqueous phase monomers used during IP.

Motivated by the immense potential of the linear aliphatic amino additives used during IP for improving the performance of the desalination membranes, we designed the current research work to investigate the impact of ethylenediamine-monoboc (EDA-Boc) on the MPD/TMC polyamide membrane. A further objective of the work was to carry out in-situ Boc-deprotection of the membrane and study its impact on the desalination potential of the resultant membranes. To achieve the above-mentioned objectives, one of the amino groups of the EDA was stoichiometrically protected while the other amino group was left free. The free amino group of EDA-Boc effectively took part in reacting with the acid chloride functional group of the TMC resulting in the covalent decoration of the EDA-Boc in the membrane. Once the EDA-Boc was bonded chemically to the membrane active layer, its Boc groups were removed on treatment with acid. The purpose of acid-based deprotection of Boc was to generate hydrophilic quaternary ammonium groups on the surface of the membrane with the potential for enhanced permeate flux and salt rejection. The existence of the EDA-Boc/MPD/TMC in the membrane active layer was verified by several characterization techniques. Other features of the membranes were also explored by membrane characterization techniques. The desalination performances of the MPD/TMC-EDA-Boc and MPD/TMC- EDA-Deboc membranes were compared with the control MPD/TMC membrane.

Results and discussion

Membranes fabrication and characterization

The Fig. 1 shows the possible reactions leading to MPD-TMC and MPD-TMC-EDA-Boc active layers decorated on the polymeric support. Once the EDA-Boc is incorporated in the membrane active layer, it can be readily deprotected leading to the generation of hydrophilic functional groups on the membrane. The possible reaction of Boc-deprotection and generation of ammonium ions in the membrane active layer is given in the Fig. 1. Hence, the current study was aimed at decorating the membrane active layer with such a molecule that can be in situ tuned resulting in enhancing the performance of the membranes in terms of permeate flux and antifouling potential while keeping the rejection considerably high.

MPD-TMC, TMC-EDA-Boc, and MPD-TMC-EDA-Deboc membranes were characterized by several techniques. ATR-FTIR analysis is shown in Fig. 2. Owing to the thin active layer and limited detection capability of the FTIR technique, the FTIR analysis was carried out for the free-standing active layers which were synthesized under the same conditions that were used for the fabrication of the membranes. In the case of the MPD-TMC active layer, several functional groups were observed which include N-H stretching vibrations located in the range of 3400 cm^{-1} followed by the peaks located at around 3000 cm^{-1} which are attributed to the aromatic -C-H stretching of the benzene rings of MPD and TMC[19]. It is important to note that upon Boc-deprotection, a broad peak of the N-H functional groups was observed in the case of the MPD-TMC-EDA-Deboc active layer. This observation confirmed the fact that the Boc-deprotection has resulted in a change in the amine functions in the active layer which can enhance the hydrophilicity of the membrane. Similarly, other peaks related to carbonyl groups of the amide linkage (-CONH) can be found in the active layer located at around 1600 cm^{-1}.

To further establish the structure of the membranes, we carried out solid-state ^{13}C NMR measurements of the free-standing active layers of the MPD-TMC-EDA-Boc (Fig. 3a) and MPD-TMC-EDA-Deboc (Fig. 3b) active layers of the membranes. The MPD-TMC-EDA-Boc membrane possessed small peaks located at 19.7 ppm, 32.1 ppm, and 38.1 ppm corresponding to the carbon atoms of the Boc and EDA. The peaks spanning from 106.6 ppm to 138.6 ppm can be attributed to the aromatic carbon atoms of the polyamides due to MPD/TMC while the peak at 155.3 ppm can be attributed to the carbonyl (> C = O) group of the amide linkage of the polyamide network. After Boc-deprotection, the peak due to Boc is completely absent in the NMR spectrum of the MPD-TMC-EDA-Deboc membrane. The peaks located at the aliphatic region of 19 to 38 ppm shifted

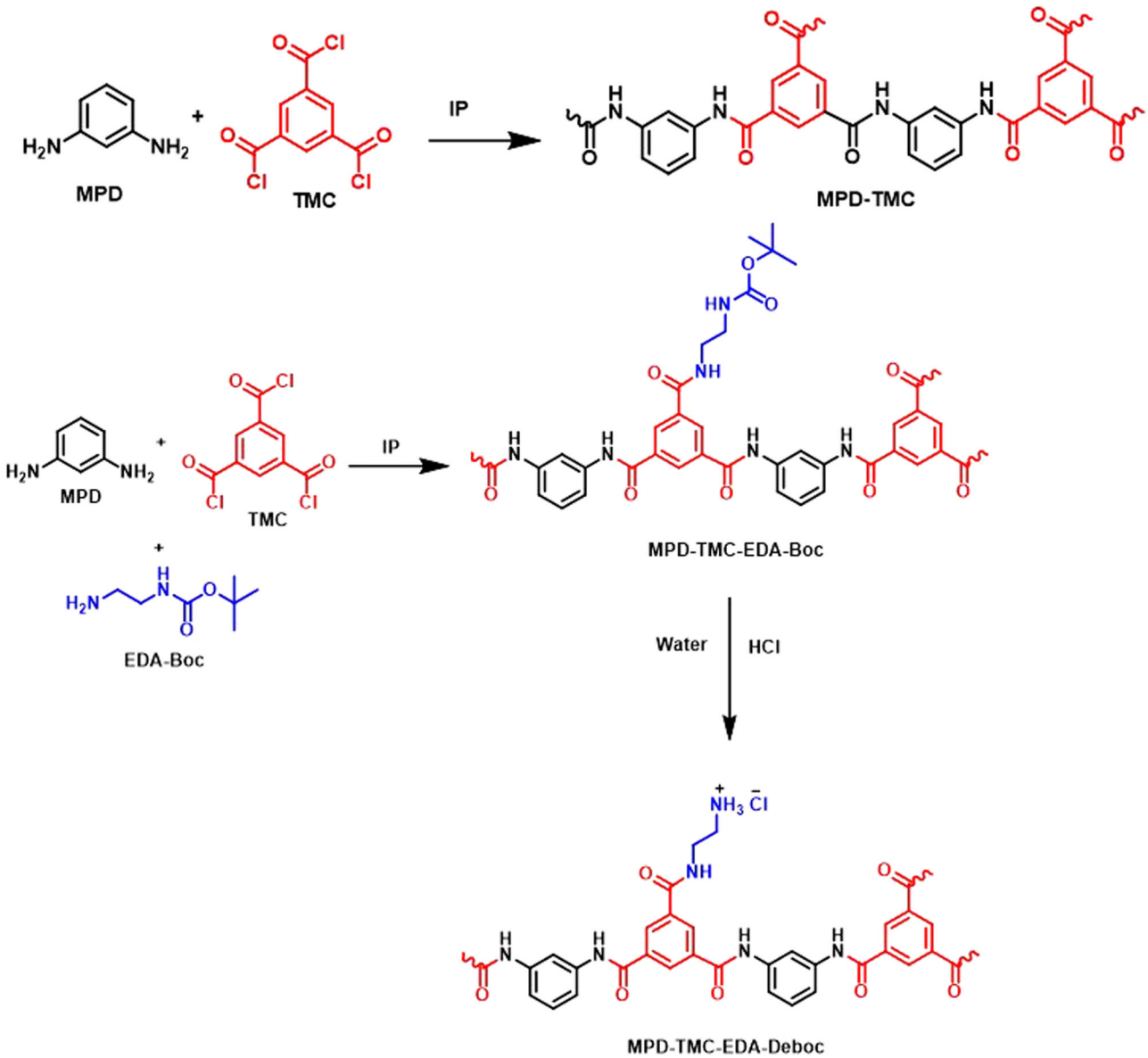

Fig. 1 | The possible reactions, active layers of MPD/TMC and MPD-TMC-EDA-Boc active layers, and Boc-deprotection in the case of MPD-TMC-EDA-Deboc active layers.

and merged with the peaks of the aromatic region, which can be attributed to the protonation of the amino groups yielding ammonium ions. Owing to the positive charge on N atoms of the ammonium ions, the carbon atoms of the EDA are more deshielded, and hence the peaks are shifted and merged with aromatic peaks. However, the other peaks such as the peaks previously identified in the MPD-TMC-EDA-Boc membrane remained intact including the carbonyl peak. These findings suggested that the Boc groups were successfully removed from the active layer yielding quaternary ammonium ions in the membrane active layer.

The variation in the chemical compositions of the active layers of the membranes is obvious and is a representation of the chemical changes brought about due to the incorporation of EDA-Boc and subsequent Boc-deprotection. The percentage of each element changed across all the membranes where the carbon percentage increased from MPD-TMC to MPD-TMC-EDA-Boc to MPD-TMC-EDA-Deboc. This increase in the percentage of C can be attributed to the presence of EDA-Boc which contains more C than oxygen and nitrogen. This fact can also be observed in decreased concentrations of O and N in the MPD-TMC-EDA-Boc and MPD-TMC-EDA-Deboc membranes. The highest variation in the composition of membranes was observed for the MPD-TMC-EDA-Deboc membrane where the C was 68 ± 0.5%, and O was reduced to 15 ± 0.5%. The decrease in the percentage of O can be attributed to the loss of tert-butoxy groups owing to Boc-deprotection. The percentage of N was observed to be 13.7% in the case of MPD-TMC-EDA-Deboc membrane which might be attributed to two reasons which are Boc-deprotection causing readjustment of elemental composition whereas the second reason is the addition of chloride ions (Cl^-) as counter ions of the ammonium ions. Additional evidence for ammonium ions was also obtained by CHNS analysis of the active layers of MPD-TMC-EDA-Boc and MPD-TMC-EDA-Deboc membranes. The CHNS analysis revealed that the percentage of hydrogen (H) was increased from 5.1% to 5.4% for MPD-TMC-EDA-Boc and MPD-TMC-EDA-Deboc membranes, respectively. These slight variations of elemental composition agree with the composition of the reaction mixture because the concentration of EDA-Boc was low during IP.

Since the polyamide active layer is grown as a crosslinked network, the degree of crosslinking was also calculated for all the fabricated membranes as given in Table 1. A minor variation in the degree of crosslinking was observed from MPD-TMC to MPD-TMC-EDA-Boc and MPD-TMC-

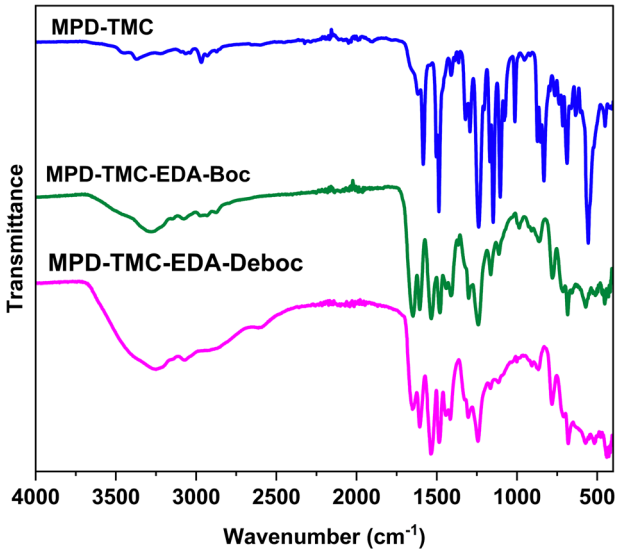

Fig. 2 | FTIR spectra of MPD-TMC, MPD-TMC-EDA-Boc, and MPD-TMC-EDA-Deboc free-standing active layers.

EDA-Deboc membranes. To avoid interference from the membrane supporting layers, the degree of crosslinking was calculated by using free-standing active layers of all membranes that were fabricated under similar conditions that were used for membrane fabrication. The degree of crosslinking of the membrane was calculated by elemental analysis by using the set of equations from 1 to 3[18] which are generally used for MPD/TMC reactions.

$$\text{Crosslinking Degree}(\%) = \frac{X}{X+Y} \times 100 \quad (1)$$

$$X + Y = 1 \quad (2)$$

$$O/N = \frac{3X+4Y}{3X+2Y} \quad (3)$$

Where "X" represents the crosslinked parts of the polyamide while "Y" represents the linear fractions of the polyamide active layer of the membrane, and 'O/N' is the Oxygen/Nitrogen ratio found by elemental analysis.

Following the determination of the structure and variations in the chemistry of the active layers, we proceeded further to investigate the other features of the membranes which included surface morphology analysis, cross-sectional studies, elemental composition, surface roughness, and wettability of the membrane surface. For surface SEM analysis, an appropriate area of each membrane was subjected to SEM analysis as shown in Fig. 4. The surface morphology analysis of the MPD-TMC membrane revealed the existence of a polyamide active layer where the polyamide chains were arranged in the form of a network with valleys in between the ridges (Fig. 4a–c). A variation in the surface morphology was observed in the case of the MPD-TMC-EDA-Boc membrane where the SEM micrographs (Fig. 4d–f) showed the existence of a relatively smoother surface having the presence of a fine polyamide active layer. The altered surface morphology can be attributed to the reaction of the EDA-Boc amine with some of the acid chloride groups in TMC which results in a different growth of the polyamide active layer than typical MPD/TMC morphology. These observations are obvious as a minor variation in the chemistry of the participating monomers induces major changes in the structure of the membrane which eventually results in changes in the performance of the membrane. On moving further to the MPD-TMC-EDA-Deboc membrane, a completely different surface morphology was observed. The surface SEM micrographs of the MPD-TMC-EDA-Deboc membrane revealed the reappearance of a more refined ridge and valley network of the polyamide (Fig. 4g–i). The Boc-

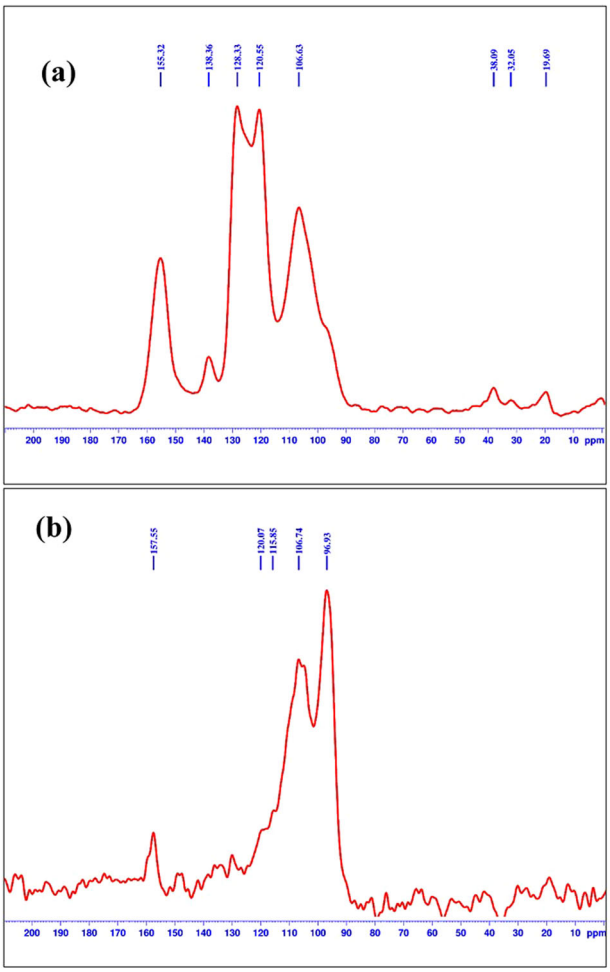

Fig. 3 | NMR analysis of the membrane active layers. Solid state ^{13}C-NMR spectra of (**a**) MPD-TMC-EDA-Boc and (**b**) MPD-TMC-EDA-Deboc membranes.

deprotection of the MPD-TMC-EDA-Boc membrane led to the generation of a fine, dense, and uniform network. Compared to the MPD-TMC control membrane, the ridges are sharper with relatively deeper valleys for the MPD-TMC-EDA-Deboc membrane. This can be attributed to the fact that the treatment of the MPD-TMC-EDA-Boc membrane with 20% HCl led to the removal of the bulky Boc groups along with all oligomers generated during the IP process. This led to the generation of a rougher membrane surface. Hence, the comparison of the SEM micrographs of the membranes confirmed the expected variation in the structural features of the membranes which has resulted in a variation in the performance of the membranes during desalination experiments.

Cross-sectional SEM analysis of the membranes was also carried out. Different magnifications of the cross-sectional SEM micrographs of all the fabricated membranes MPD-TMC (Fig. 5a–c), MPD-TMC-EDA-Boc (Fig. 5d–f), and MPD-TMC-EDA-Deboc (Fig. 5g–i) are presented. An intact asymmetric membrane structure was observed for all three membranes where the lowest layer represents the nonwoven fabric (PET), the middle layer is PSF UF support, and the top layer is the polyamide active layer of the membranes. This asymmetric structure is an essential structural feature of the membranes which is essential for desalinating the salts present in the feed and provides free passageways to the permeating water molecules through the membranes. The active layer is a highly dense skin layer having extremely fine pores that separate the salts from the permeating water owing to size exclusion in addition to other mechanisms involved in desalting the water. The thickness of the active layers of the membranes was measured by ImageJ software where the thickness was found to be varied from one membrane to another. The thickness of the polyamide active layers for

Table 1 | The elemental composition of the active layers of all three membranes and the degree of crosslinking

Membranes	C	O	N	Cl	O/N ratio	X[a]	Y[b]	Degree of crosslinking (%)
MPD-TMC	62.9	19.9	17.1	0	1.16	0.778	0.222	77.8
MPD-TMC-EDA-Boc	67.9	17.0	15.0	0	1.13	0.817	0.183	81.7
MPD-TMC-EDA-Deboc	68.8	15.3	13.7	2.1	1.12	0.830	0.170	83.0

[a]The crosslinked part of the polyamide active layer.
[b]The linear part of the polyamide active layer of the membrane.

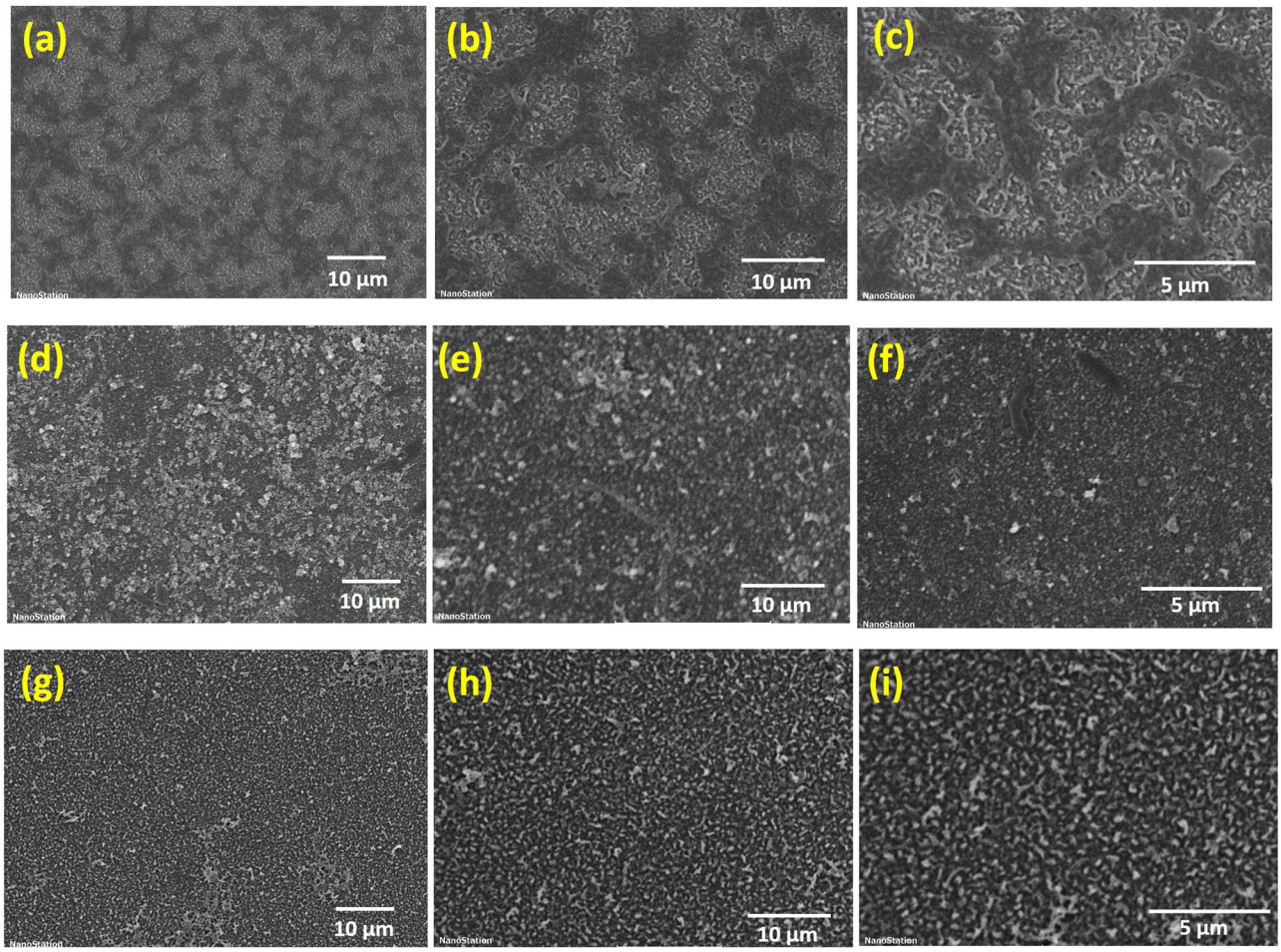

Fig. 4 | Surface SEM analyses of the fabricated membranes. SEM micrographs showing the surface morphology of MPD-TMC (**a**–**c**); MPD-TMC-EDA-Boc (**d**–**f**); and MPD-TMC-EDA-Deboc (**g**–**i**) membranes at different magnifications.

MPD-TMC, MPD-TMC-EDA-Boc, and MPD-TMC-EDA-Deboc was found to be 145 nm, 244 nm, and 187 nm, respectively. Therefore, on Boc-deprotection, the thickness of the membrane was decreased which could result in reduced mass transfer resistance during filtration and passage of the feed through the membrane. The PSF UF support possesses several finger-like projections which can be attributed to the non-solvent-induced phase inversion/separation (NIPS) where the solvent DMAc is rapidly de-mixed from the polymer matrix and dissolves into water. These finger-like projections offer free channels for the unhindered transport of permeating water molecules through the membrane.

The elemental composition of the membranes was determined by EDX analysis of the membranes (Fig. 6). A similar composition to that of the free-standing active layers having C, N, and O was observed for all the membranes structure.

The mapping analysis of the membrane also confirmed the uniform distribution of all the elements that were found in the membranes (Fig. 7). The intensity of the dots in each map is related to the concentration of that element in the membrane structure where carbon being the most abundant has the highest intensity of the C atoms in the map followed by O and N. The concentration of C and N is almost the same whereas O is slightly more concentrated compared to N. Normally, a N:O of 1 is expected for the completely crosslinked polyamide network confirming that each N is part of the amide bond (-CONH) and linked to the O atom of the >C = O group of the amide bond. Hence, in an ideal situation, the concentration of N should be equal to that of O but in the polyamide active layer certain acid chloride groups are also hydrolyzed during IP upon exposure to the aqueous medium and hence the concentration of O is slightly more than that of N. This fact has also been observed in the elemental composition of the free-standing active layers of the membranes. Moreover, the membrane's bulk porosity was also calculated using the given Eq. (4)[20]. The membrane's bulk porosity was

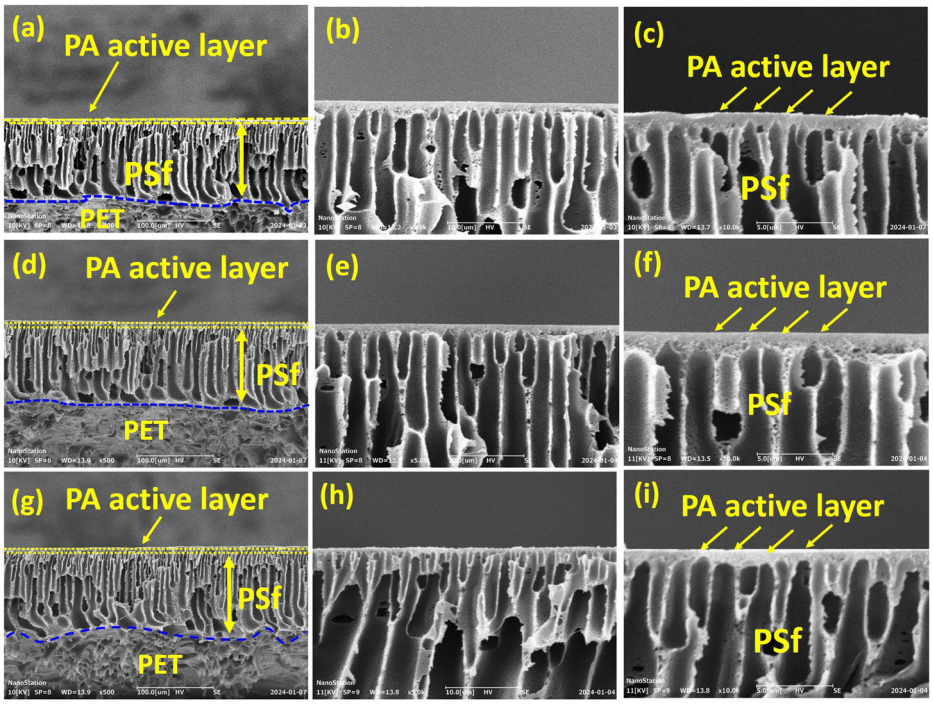

Fig. 5 | Cross-sectional SEM analyses of the fabricated membranes. Cross-sectional view of membranes MPD-TMC (**a**–**c**); MPD-TMC-EDA-Boc (**d**–**f**); and MPD-TMC-EDA-Deboc (**g**–**i**) at varying magnifications.

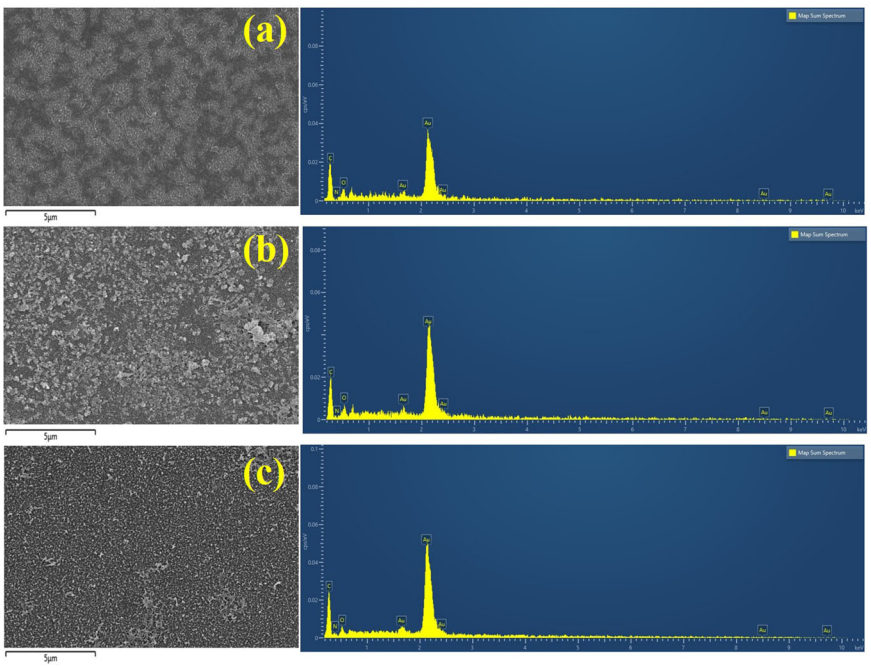

Fig. 6 | EDX analyses of the fabricated membranes. EDX spectra of MPD-TMC (**a**); MPD-TMC-EDA-Boc (**b**); and MPD-TMC-EDA-Deboc (**c**) membranes.

determined to be 9.6, 5.7, and 6.6% for MPD-TMC, MPD-TMC-EDA-Boc and MPD-TMC-EDA-Deboc membranes, respectively.

$$\varepsilon(\%) = \frac{W_{wet} - W_{dry}}{V\rho_w} \times 100 \quad (4)$$

Where W_{wet}, and W_{dry} are the wet and dry weights of the membrane in kg, V is the volume of the dry membrane in m^3 and ρ_w is the density of the water in kg m^{-3}.

Another extremely important feature of the membranes is the surface roughness which contributes to several factors such as surface wettability and membrane surface fouling during filtration experiments. The surface roughness of the membranes was determined by atomic force microscopy (AFM) analysis of the membranes. The 2D and 3D AFM images of the membranes are given in Fig. 8. As depicted by the SEM surface micrographs of the membranes, the MPD-TMC-EDA-Boc (Fig. 8b) membrane appeared smoother compared to the MPD-TMC (Fig. 8a) and MPD-TMC-EDA-Deboc (Fig. 8c) membranes. An average surface roughness (R_a) of 6.3 nm was recorded for MPD-TMC-EDA-Boc membranes compared to 7.3 nm for MPD-TMC and 7.9 nm for MPD-TMC-EDA-Deboc membranes. Moreover, the reaction of the MPD and TMC can also be possibly impacted to a certain extent as some

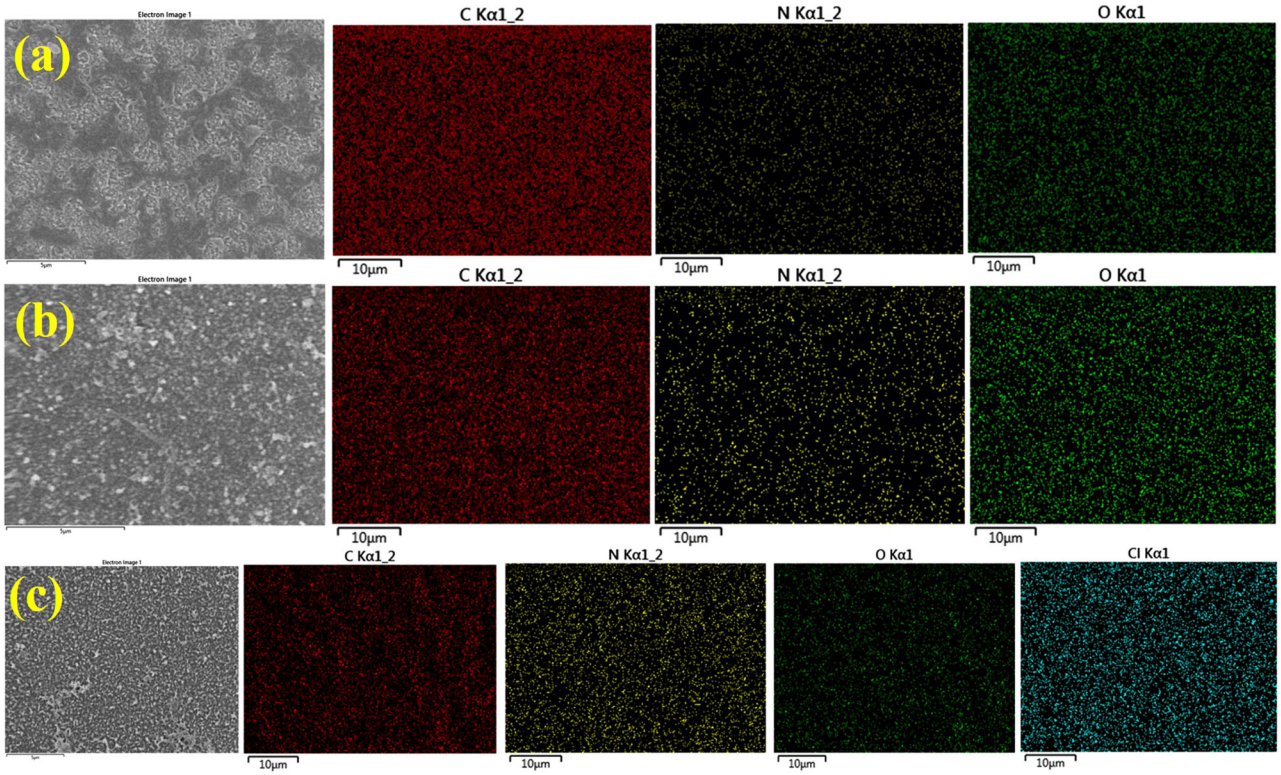

Fig. 7 | Mapping analyses of the fabricated membranes. Elemental mapping images of MPD-TMC (**a**); MPD-TMC-EDA-Boc (**b**); and MPD-TMC-EDA-Deboc (**c**) membranes showing the distribution of surface elements.

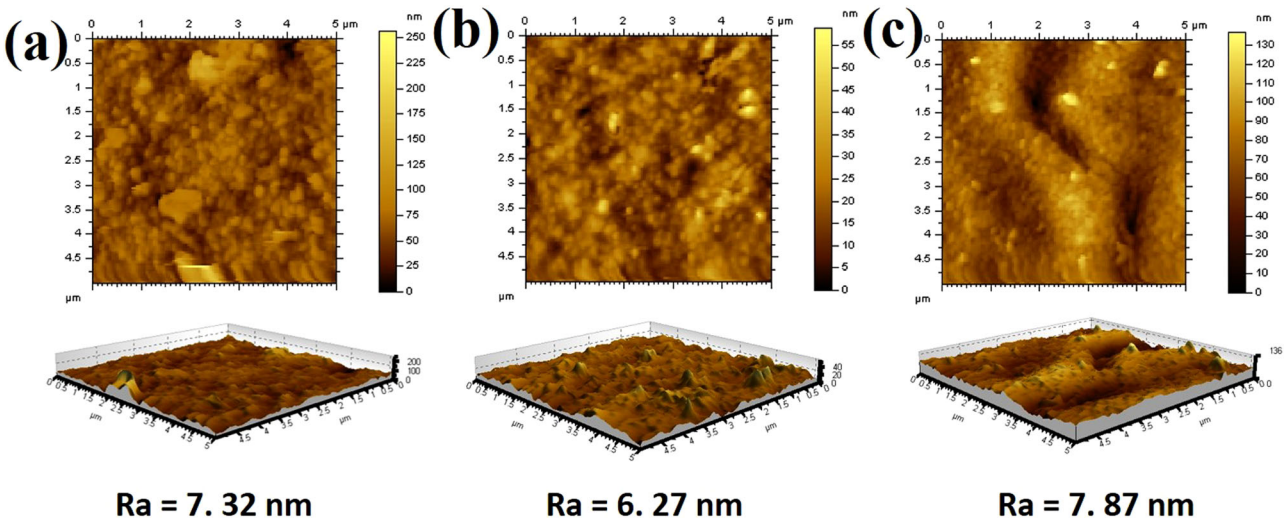

Fig. 8 | Surface roughness analyses of the membranes by atomic force microscopy. 2D and 3D AFM microscopic images of (**a**) MPD-TMC, (**b**) MPD-TMC-EDA-Boc and (**c**) MPD-TMC-EDA-Deboc illustrate the surface roughness of prepared membranes.

of the sites of the TMC are covered by EDA-Boc which eventually impacts the way of growth of the polyamide active layer during IP. However, upon Boc-deprotection, the *tert*-butoxy groups are removed from the polyamide active layer coupled with the removal of certain oligomers yielding a rougher membrane surface as has been observed in the case of MPD-TMC-EDA-Deboc membrane. These surface roughness values of the membranes agree with the surface morphologies observed for the membranes during SEM analysis.

Another closely related feature is the membrane's surface wettability which affects the performance of the membranes such as the antifouling potential and permeability. The wettability of a membrane depends on several factors such as chemistry, the active layer, and the surface roughness of the membrane. Generally, the membrane surface wettability is determined by the water contact angle (WCA) of the membranes where the lowering of WCA value is associated with increasing the hydrophilicity of the membrane and vice versa. Generally, Young's model considers the fact that the increase in membrane surface roughness causes an increase in its surface wettability. On the other hand, the Wenzel model considers the fact that a decrease in membrane surface roughness causes a decrease in the water contact angle (WCA) of the membrane which has also been observed in literature[21,22]. In the current scenario, this relationship between surface roughness and hydrophilicity is true only when we move from the MPD-TMC membrane to MPD-TMC-EDA-Boc as the surface roughness is decreased from 7.3 nm to 6.3 nm. Hence, the WCAs for MPD-TMC and

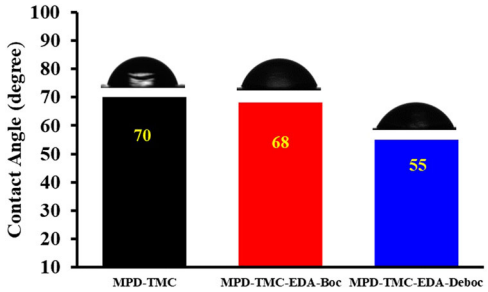

Fig. 9 | Contact angle measurements of prepared membranes.

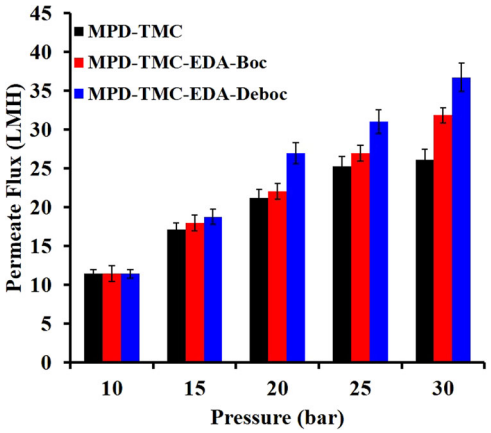

Fig. 10 | Effect of feed pressure on the permeate flux of the fabricated MPD-TMC, MPD-TMC-EDA-Boc, and MPD-TMC-EDA-Deboc membranes using deionized water as feed where the membranes are installed in parallel on a crossflow filtration system. The error bars show the standard deviation ($n = 3$).

MPD-TMC-EDA-Boc membranes were measured to be 70.0° and 68.0° (Fig. 9). However, in the case of the MPD-TMC-EDA-Deboc membrane, the surface hydrophilicity increases (WCA = 55.0°) with an increase in the membrane surface roughness ($R_a = 7.87$ nm). This observation highlights the fact that the surface roughness of the membrane is not the only contributing factor in controlling the wettability of the membrane, the chemistry of the membrane plays a significant role in determining the surface wettability of the membranes. The MPD-TMC-EDA-Deboc membrane has an altered membrane chemistry owing to the generation of hydrophilic ammonium ions on the surface of the membrane. The additional hydrophilic functionality on the membrane surface results in the lowering of the WCA of the membrane resulting in increased surface hydrophilicity.

Desalination performance of the membranes

Following characterization and establishing the structural features of the membranes, the performance of the membranes was evaluated. Initially, the effect of feed pressure on the permeate flux was measured by using DI water as feed while the membranes were installed in parallel on a crossflow filtration system. An obvious increase in permeate flux was observed with an increase in feed pressure (Fig. 10). The control MPD/TMC membrane was measured to have the lowest flux compared to the two other membranes. The highest pressure applied in the current study was 30 bar where a greater permeate flux was observed for the MPD-TMC-EDA-Boc (33.0 ± 0.5 L m^{-2} h^{-1}) and MPD-TMC-EDA-Deboc (37.0 ± 0.2 L m^{-2} h^{-1}) membranes compared to the MPD-TMC membrane (26.0 ± 0.2 L m^{-2} h^{-1}) (Fig. 10). This increase in permeate flux from MPD-TMC to MPD-TMC-EDA-Deboc membrane is anticipated from the structure of the membranes. The MPD-TMC control membrane possesses a normal polyamide network having only amide linkage (>CONH) as the hydrophilic functional group of the membrane whereas the other component is a hydrophobic benzene ring. On the other hand, the

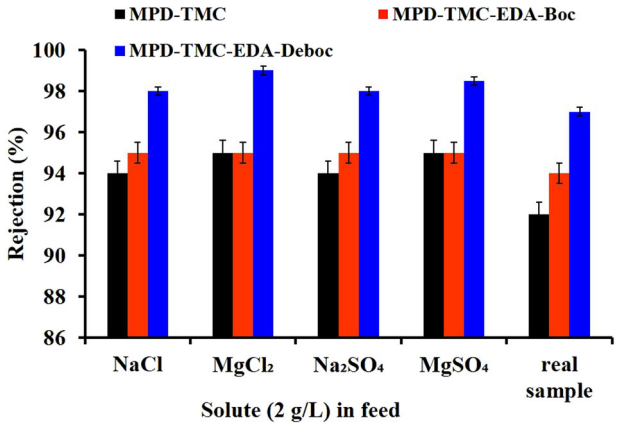

Fig. 11 | The rejection performance of the mono, divalent ions, and the seawater NF permeate by the three fabricated membranes; MPD-TMC, MPD-TMC-EDA-Boc, and MPD-TMC-EDA-Deboc at 20 bar. The error bars show the standard deviation ($n = 3$).

MPD-TMC-EDA-Boc membrane has not only additional amide linkages but also a linear aliphatic component (EDA-Boc) which enhances the hydrophilicity and causes a slight increase in the flexibility of the polyamide active layer of the membrane. Hence, the MPD-TMC-EDA-Boc membrane demonstrated a higher permeate flux. In the case of the MPD-TMC-EDA-Deboc membrane, the generation of ammonium ions on the membrane develops a strong hydration layer owing to interaction with the water molecules which in turn causes an increase in the permeate flux of the membrane. Furthermore, the WCA measurements of the membranes also revealed that the MPD-TMC-EDA-Deboc membrane has the lowest WCA (55°) among all the fabricated membranes. This lowering of WCA reflects an increase in hydrophilicity which eventually results in increased permeate flux. Hence, the membrane surface chemistry is crucial in contributing to the flux enhancement of the membrane. Despite a slight increase in the degree of crosslinking from MPD-TMC to MPD-TMC-EDA-Deboc membrane, the flux has increased which further confirms the fact that the permeate flux is governed by multiple factors including membrane surface wettability, chemical structure, and crosslinked physical network.

Following measurements of permeate flux, another important parameter is the measurement of the rejection of the salts by the fabricated membranes. The rejection of both monovalent (NaCl) and divalent salts ($MgCl_2$, Na_2SO_4, and $MgSO_4$) was measured by using the fabricated membranes at a pressure of 20 bar (Fig. 11). The rejection of NaCl stayed >93% for all the fabricated membranes including the control MPD-TMC membrane. In comparison to the control MPD-TMC membrane, the MPD-TMC-EDA-Boc and MPD-TMC-EDA-Deboc membranes showed higher NaCl rejection. A NaCl rejection of $95 \pm 0.5\%$ was measured for the MPD-TMC-EDA-Boc membrane while it was further increased to $98 \pm 0.5\%$ for the MPD-TMC-EDA-Deboc membrane. The rejection of divalent salts was measured to be >95% for all the membranes whereas again the MPD-TMC-EDA-Deboc membrane showed the highest salt rejection (>98%) among all the fabricated membranes. Among all the salts studied in the current work, $MgCl_2$ was the most rejected salt, having a rejection of 99% (Fig. 11). Like flux, the rejection of salts by the membrane involves several mechanisms which include size exclusion, the crosslinked polyamide network, surface charge/charge exclusion, solution diffusion, and advective transport of salts through the membrane[23,24]. As far as the size exclusion is concerned, the hydrated monovalent ions being smaller in size can readily pass through the membrane compared to bigger salt ions. Therefore, the difference between the rejection of monovalent and divalent salts can be described by simply considering the size exclusion principle. Now as we consider the divalent salts, $MgCl_2$ was measured to have the highest rejection among all the tested salts which can be explained by considering several factors such as the size, charge, and number of ions per molecule. Magnesium has a charge of +2

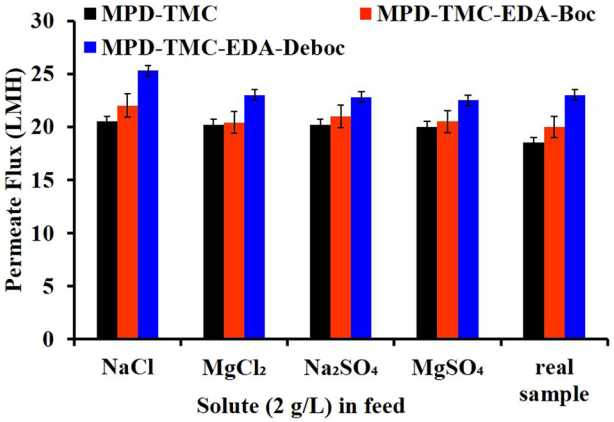

Fig. 12 | Comparative filtration data of three membranes at fixed solute concentration and 20 bar pressure. The error bars show the standard deviation ($n = 3$).

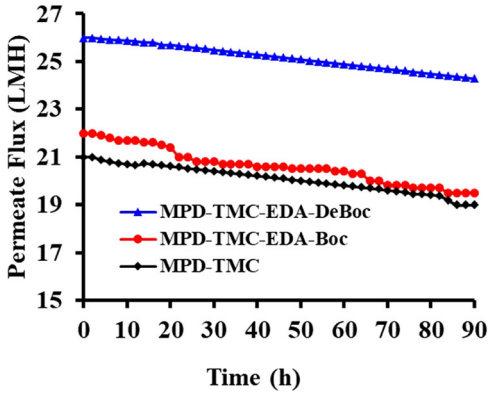

Fig. 13 | Variation of permeate flux with time for the membranes for representative experiments in the presence of fouling agent (bovine serum albumin), at 20 bar.

and a bigger hydration radius compared to Na^+ (0.86 nm cf. 0.72 nm). Similarly, SO_4^{-2-} has a greater hydration radius than Cl^- (0.76 nm cf. 0.66 nm)[25,26]. Hence, considering the hydration radii of the ions, salts such as $MgSO_4$ are expected to have the highest rejection. A rejection of 98.5 ± 0.5% was measured for $MgSO_4$ which is comparable to the rejection of $MgCl_2$ (99.0 ± 0.5%). The slightly higher rejection of $MgCl_2$ can be attributed to not only the hydration radius but also to the number of ions being rejected. In the case of $MgCl_2$, three ions per molecule are rejected by the membrane under filtration conditions. The rejection of Na_2SO_4 (98.0 ± 0.5%) is comparable to that of NaCl (98%) which highlights a significant observation that the rejection of the salts depends more on the nature of the ions involved in addition to the charge on the ions[27]. The higher salt rejection performance of the MPD-TMC-EDA-Deboc membrane can be attributed to the presence of positively charged ammonium ions on the surface of the membrane due to the Deboc of the EDA groups. A repulsive force exists between the ammonium ions on the surface of the membranes and cations such as Na^+ and Mg^{2+} present in the feed leading to higher salt rejection. The increasing degree of crosslinking (Table 1) from MPD-TMC to MPD-TMC-EDA-Boc and MPD-TMC-EDA-Deboc membranes is also a contributing factor to increasing the rejection of salts by the membrane. In addition, the decrease in bulk porosity of the MPD-TMC-EDA-Deboc membrane can also result in higher rejection rates since less number and narrower pathways are available for the penetration of the salts. This is attributed to the increased resistance provided by the narrow channels of the polyamide framework of the membranes. Therefore, altering the active layer chemistry impacts the chemical and physical structure of the membrane which eventually results in varied desalination performance of the membrane. For the sake of comparison, the seawater NF permeate at a TDS level of 33,700 ppm was collected from the permeate of the NF membrane, and the desalination potential of the fabricated membranes was explored. The MPD-TMC-EDA-Deboc membranes showed a rejection rate of 97%, while the MPD-TMC-EDA-Boc membrane had a rejection rate of 94%, and the MPD-TMC membrane rejected 92% of the TDS.

Following the salt rejection, we also studied the pure water permeate flux of different salt-containing feeds at a constant transmembrane pressure of 20 bar. In comparison to DI water used as feed, the permeate flux of the salt-containing feeds was lower (Fig. 12). In the case of DI water feed, the permeate flux was recorded to be 22 ± 0.5 L m^{-2} h^{-1}, 23 ± 0.5 L m^{-2} h^{-1}, and 27 ± 0.5 L $m^{-2}h^{-1}$ for MPD-TMC, MPD-TMC-EDA-Boc and MPD-TMC-EDA-Deboc membranes, respectively. However, with NaCl as feed, the permeate flux was recorded to be 25 ± 0.5 L m^{-2} h^{-1} for the MPD-TMC-EDA-Deboc membrane. A further decrease in permeate flux was recorded in the case of divalent salts such as $MgCl_2$ and $MgSO_2$. Hence, the nature of the salt impacts not only the salt diffusion but also the permeate flux. If we closely observe the permeate flux profiles of the different salt-containing feeds, it can be observed that the permeate flux in the case of NaCl is more (25 ± 0.5 L m^{-2} h^{-1}) than that of Na_2SO_4 (23 ± 0.5 L m^{-2} h^{-1}). Similarly, the permeate flux of $MgCl_2$ is slightly more (23.5 ± 0.5 L m^{-2} h^{-1}) than that of $MgSO_4$ (23 ± 0.5 L m^{-2} h^{-1}) for the MPD-TMC-EDA-Deboc membrane. This observation suggests that the nature of the anions present in the feed affects the permeate flux of the MPD-TMC-EDA-Deboc[27]. These results can be explained because the MPD-TMC-EDA-Deboc membrane possesses positively charged ammonium ions decorated on the surface of the membrane which develops strong repulsion for the cations while anions are attracted towards the membrane surface. The attachment of the anions on the membrane surface results in a lowering of the permeate which is also reflected by the lower NaCl rejection. The attachment of the anions on the membrane surface provides a shielding effect and hence the membrane does not remain repulsive to Na^+ which owing to its smaller hydration radius passes through the membrane under higher feed pressure. In the case of seawater NF permeate, the permeate flux showed a slight decline which is well anticipated owing to concentration polarization (CP). The MPD-TMC-EDA-Deboc membranes showed a permeate flux of 23 L m^{-2} h^{-1}, MPD-TMC-EDA-Boc membranes possessed a permeate flux of 20 L m^{-2} h^{-1} and the MPD-TMC membrane had a permeate flux of 18.5 L m^{-2} h^{-1} for the seawater NF permeate.

The study was further extended by including another important parameter related to the performance of the membrane which is the anti-fouling potential of the membrane. The desalination membranes are fed with a feed after several pretreatment steps which minimize the evidence of membrane fouling. However, it has been observed that membrane fouling is an inevitable process whether it is biofouling, inorganic, or organic fouling on the membrane surface. In the current study, 200 ppm BSA solution was used as feed to simulate the proteinaceous organic foulants found in seawater. The BSA feed was run for 6 continuous hours in a crossflow mode at 20.0 bar which resulted in a decrease in the permeate flux of the membranes. This decrease in permeate flux was greater initially, then gradually stabilized and remained plateaued. The rapid decrease in permeate flux of the membrane during the initial stages of the fouling experiments is obvious due to the abundant availability of the attachment sites for foulants at the surface of the membrane. Hence, the foulants are rapidly attached to the membrane surface while with time the attachment sites are not available for further attachment leading to a plateaued performance of the membrane during later stages of the fouling experiments. The flux decreased from 21.0 ± 0.5 L m^{-2} h^{-1} to 19.0 ± 0.5 L m^{-2} h^{-1} for the MPD-TMC membrane and a decrease of 22.0 ± 0.5 L m^{-2} h^{-1} to 19.0 ± 0.5 L m^{-2} h^{-1} was observed for MPD-TMC-EDA-Boc membrane (Fig. 13). In the case of MPD-TMC-EDA-Deboc membrane, a larger decrease in permeate flux was observed where the permeate flux of the membrane decreased from 27.0 ± 0.5 L m^{-2} h^{-1} to 24 ± 0.5 L m^{-2} h^{-1}. Although the MPD-TMC-EDA-Deboc membrane possesses a relatively more hydrophilic surface, foulants like BSA also have several charged groups that develop interactions with the membrane's active layer. BSA is a protein that is composed of amino acid chains

crosslinked through several disulfide bonds and hence BSA has both hydrogen bond donors and acceptor groups such as >C = O, -NH, -CONH, NH_2, -COOH, and -SH groups which could develop interactions with the membrane.

After studying the fouling behavior of the membrane, our next objective was to use a cleaning protocol for making the membranes reusable. For this sake, we backwashed the membrane using DI water at 20 bar for 1 h and the results are demonstrated in Fig. 14. As we know all the membranes underwent minor fouling during the 6 h of fouling test with BSA and the flux decline of 10%, 11%, and 12% was observed for MPD-TMC, MPD-TMC-EDA-Boc, and MPD-TMC-EDA-Deboc, respectively. Although the MPD-TMC-EDA-Deboc membrane has more fouling compared to that of the other two membranes, it also demonstrated the largest flux recovery of 95.0 ± 0.5% of its original flux. Hence, the hydrophilic surface of the MPD-TMC-EDA-Deboc membrane favors the removal of loosely held foulants owing to the stronger sheer force of the water molecules resulting in cleaning the membrane surface.

The desalination performance of the MPD-TMC-EDA-Deboc membrane was compared with similar membranes. It was found to be among the most promising in terms of permeate flux and salt rejection. This method is notably advantageous as it relies on the covalent bonding of EDA-Boc in the membrane's active layer, thereby avoiding issues such as inhomogeneity and defects caused by inorganic fillers like TiO_2 in the organic polyamide layer. Table 2 provides comparative data showing the performance of the MPD-TMC-EDA-Deboc membrane alongside other RO membranes reported in the literature.

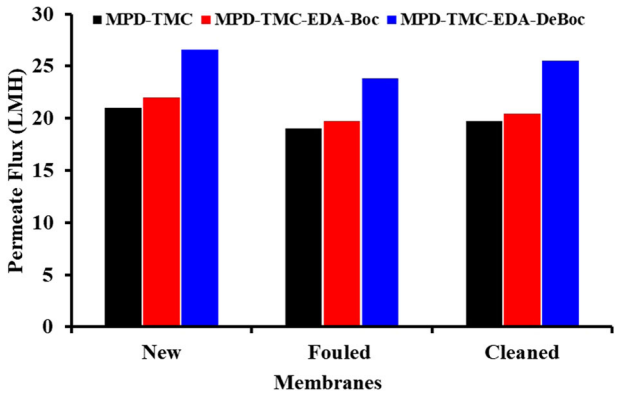

Fig. 14 | Variation in permeate flux observed after backwashing of fouled membranes, at 20 bar.

Interestingly, tuning the active layer chemistry of the polyamide membranes has demonstrated enhancement in the desalination potential of the polyamide thin film composite membranes. The in-situ Boc-deprotection of the EDA-Boc by using 20% HCl solution led to the generation of ammonium ions in the membrane active layer which was reflected by the lowering of WCA from 70° for the MPD-TMC membrane to 55° for MPD-TMC-EDA-Deboc membrane. This increase in membrane surface hydrophilicity correlated with an enhancement of the permeate flux of the membrane from 26 L m^{-2} h^{-1} for MPD-TMC membrane to 37 L m^{-2} h^{-1} MPD-TMC-EDA-Deboc membrane at 30 bar. Moreover, the salt rejection showed an increase from 94% NaCl to 98% NaCl rejection. The fouling test by using BSA feed for six continuous hours showed a minor decrease ≈ of 10% in permeate flux which was recovered up to 95% by backwashing the membranes using DI water. Hence, this work demonstrates the potential of this approach for tuning the chemistry of the membrane's active layer to enhance the desalination potential of the membranes.

Methods

Materials chemicals and reagents

Polysulfone beads (PSf, 99%), polyvinyl pyrrolidone (PVP, 99%), ethylenediamine (EDA, 98%), m-phenylenediamine (MPD, 99%), trimesoyl chloride (TMC, 99%), Di-*tert*-butyl dicarbonate (Diboc), n-hexane (99%), hydrochloric acid (97%), dichloromethane (DCM, 99%), bovine serum albumin (BSA) and dimethylacetamide (DMAc, 99%) were acquired from Sigma (USA) and used as received. Polyethylene terephthalate (PET) support (Novatexx–2413) was obtained from Freudenberg Filtration Technologies (Germany).

Characterization

Functional groups present in the membranes were analyzed using ATR-FTIR (Nicolet™ iS50, Thermo Fisher Scientific), with spectra recorded by pressing a dried membrane piece onto a polished ATR crystal. Scanning Electron Microscopy (Quattro SEM, Thermo Fisher) was employed to observe the surface morphology of membrane pieces pre-coated with a gold layer to mitigate charging artifacts. The elemental composition and spatial distribution within the membrane's active layer were investigated through SEM-coupled Energy Dispersive X-ray (EDX) analysis. Surface hydrophilicity was determined by measuring the water contact angle (WCA) of the membranes. Rectangular membrane samples (1 × 4 cm) affixed to glass slides were utilized, and WCAs were measured using a goniometer (DSA 20,

Table 2 | Comparison of MPD-TMC-EDA-Deboc membrane with other membranes reported in the literature

Membranes	Reagents used	Pure Water Flux (L m^2h^{-1})	Rejection of monovalent ions (%)	Ref.
Polyamide/PSf	*m*-phenylenediamine/trimesoyl chloride/ PF127/SDS mixed micelles	35.0	>99.0	30
Polyamide/PSf	*m*-phenylenediamine/trimesoyl chloride/aminated imidazolium/Br	30.0	98.5	31
Polyamide/PSf	*m*-phenylenediamine/trimesoyl chloride/graphene oxide	14 ± 0.3	96.4	32
Polyamide/PSf	*m*-phenylenediamine/trimesoyl chloride/TiO_2/ graphene oxide	23.6	95.3	33
Polyamide/PSf	*m*-phenylenediamine/trimesoyl chloride/formaldehyde/ glutaraldehyde	37.5	98.6	34
SW30HR, Dow Filmtech (Minneapolis, MN)	*m*-phenylenediamine/trimesoyl chloride	9 ± 0.8	98.5	35
Polyamide/PSf	*m*-phenylenediamine/trimesoyl chloride/TiO_2/SiO_2	23.0	94.0	36
Polyamide/PSf	*m*-phenylenediamine/trimesoyl chloride/Laponite nanoclays	35.0	99.0	37
Polyamide/PSf	*m*-phenylenediamine/trimesoyl chloride/Bis(3-aminopropyl) amine	45.0	93.7	4
Polyamide/PSf	MPD-TMC-EDA-Deboc	37 ± 0.2	>98.0	This work

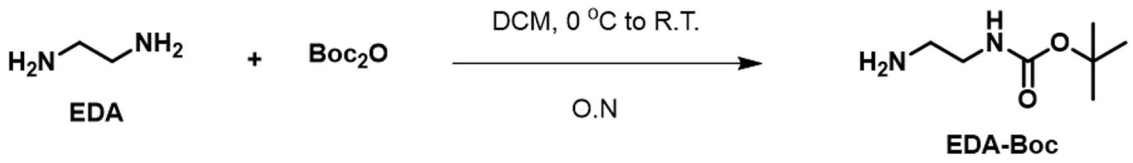

Fig. 15 | The synthesis route for the EDA-Boc.

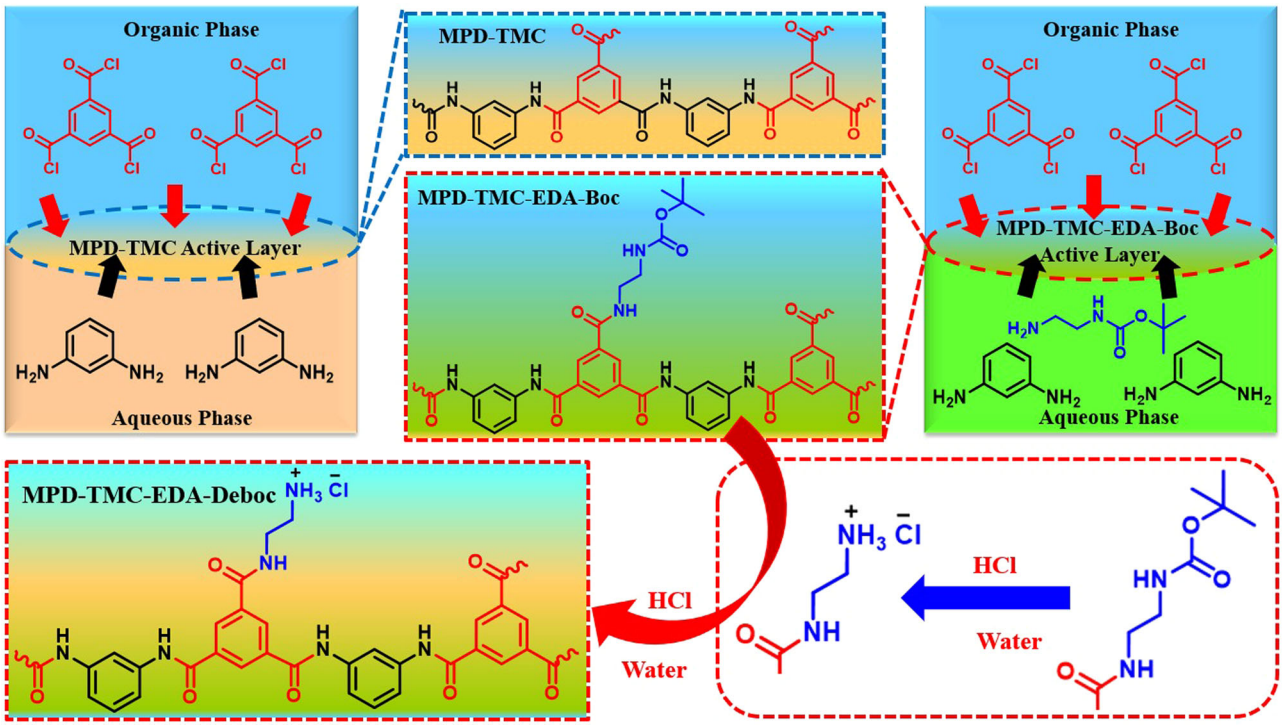

Fig. 16 | Steps and stages involved in the fabrication of membranes including control MPD-TMC, MPD-TMC-EDA-Boc, and MPD-TMC-EDA-Deboc membranes.

KRUSS GmbH). The built-in camera captured images during the placement of approximately 10 µL water droplets on the sample surface. Surface roughness was assessed using atomic force microscopy (Easy Scan 2 Nanosurf, Inc.) in tapping mode. Membrane pieces (2 × 2 cm) were securely attached to glass slides, and a scanning area of 10 × 10 µm was selected from various regions of each sample. Images were acquired in two- and three-dimensional modes and the in-built software was utilized to calculate the average roughness. Elemental analysis (CHNS/O) was performed using an elemental analyzer (Flash Smart, Thermo Scientific). Additionally, solid-state ^{13}C-NMR (CP-MAS) spectra were recorded on a Jeol-600 MHz NMR instrument (Jeol, Tokyo, Japan) to ensure the chemical structure of the active layer of the membranes.

Membrane fabrication and their testing

Initially, the protection of one amino group in the EDA monomer was achieved by introducing a Boc (tert-butyloxycarbonate) group. In this process, 9.0 ml (0.14 mol) of EDA monomer and 2.6 g (0.012 mol) of Boc were separately dissolved in 100 ml and 5 ml of dichloromethane (DCM), respectively. The Boc solution was then added dropwise to the EDA monomer solution under vigorous stirring at 0 °C and then the stirring was continued at 25 °C for 6 h, resulting in the formation of a solid product. The completion of the reaction was monitored by TLC analysis. Subsequently, the solid product was collected by evaporating the solvent using a rotary evaporator, and the obtained product was dissolved in DCM and washed with $NaHCO_3$, water, and brine. Finally, the compound was purified through a plug of silica. Figure 15 shows the synthesis route for the EDA-Boc. The characterization data especially ^{1}H and ^{13}C NMR were matched with our previously reported study[28].

For the IP reaction, two separate aqueous amine solutions were prepared, one containing MPD (2.0 wt%) and the other containing MPD (1.90 wt%) and EDA-Boc (0.10 wt%). The organic phase was prepared by preparing a solution of TMC (0.15 wt./v %) in n-hexane. TMC was used as a crosslinker during IP. The polyamide active layers were synthesized on the PSf/PET supports. A non-solvent-induced phase separation (NIPS) approach was adopted for fabricating PSf/PET supports. In a typical procedure, the dope solution of PSf (18.0 g PSf beads, 2.0 g PVP powder, 80.0 g DMAc was stirred at 70 °C until a clear solution was obtained, which was allowed to degas overnight before casting on non-woven PET support held on a glass sheet. The casting was carried out using a doctor's blade (100 µm) and immediately the cast film was dipped in a DI water bath leading to the solidification of the PSF to give the PSf/PET support. Before the IP process, the PSf/PET support was soaked in deionized water for 24 hours. During the IP reaction, the supports were separately immersed in the aqueous amine solutions of MPD and MPD + EDA-Boc for 10 min at room temperature. The amine-impregnated supports were removed from the aqueous solutions where the excess amines were removed by using a rubber roller. The amine-loaded supports were then allowed to dry at room temperature. After that, the supports were immersed separately in n-hexane solutions of TMC for 60 s leading to the fabrication of a polyamide active layer on the PSf/PET support. The fabricated membrane was removed from the TMC solution and washed with clean n-hexane to remove any unreacted TMC. Finally, the membrane was cured at 60 °C for 15 min in an air-forced oven to obtain the

final MPD-TMC control membrane and MPD-TMC-EDA-Boc membrane.

A third membrane was also prepared in the current study where the Boc group was deprotected yielding an MPD-TMC-EDA-Deboc membrane. For the sake of Boc-deprotection a procedure reported in the literature was adopted with slight modification[29], the as-prepared MPD-TMC-EDA-Boc membrane was treated with 100 ml of aqueous solution of HCl acid (20% v/v) for 6 h. The resulting MPD-TMC-EDA-Deboc membrane was then washed with deionized water to remove excess acid. For the sake of comparison, free-standing active layers of all three fabricated membranes were also synthesized by following the same conditions and protocols that were used for the fabrication of the membranes. Figure 16 illustrates the reaction steps involved in the whole synthesis procedure.

The filtration experiments were performed in a crossflow filtration system (BONA-TYLG-19; Shandong Bona Biological Technology Group Co., LTD, China) where the three membranes were installed in parallel. The membranes were compacted at 30 bar until a steady flux was achieved. The rejection of salts by the membrane was calculated using the Eq. 5:

$$\text{Rejection}\,(\%) = \left(1 - \frac{C_2}{C_1}\right) \times 100 \tag{5}$$

Where C_1 and C_2 are the conductivity (mS) of the feed and permeates, which should be proportional to the total dissolved solids content over the range of concentrations used in the experiments. The conductivity of the feed and permeate was measured using a conductivity meter (Mettler Toledo Seven Excellence™, Merck, Germany). NF-treated Arabian Gulf seawater was provided by the Saudi Water Authority for studying the real seawater feeds.

The permeate flux (J) of the membrane was measured by using Eq. 6:

$$\mathrm{J} = \frac{V}{A \times t} \tag{6}$$

Where J is the permeate flux (L m^{-2} h^{-1}) of the membranes, V denotes volume (L), t denotes time (h), and A is the membrane effective area (m2) which carries out the job of filtration.

Data availability

All data generated or analyzed during this study are included in this published article.

Received: 28 March 2024; Accepted: 10 July 2024;
Published online: 25 July 2024

References

1. Kadhom, M. A review on the polyamide thin film composite (TFC) membrane used for desalination: Improvement methods, current alternatives, and challenges. *Chem. Eng. Res. Des.* **191**, 472–492 (2023).
2. Habib, S. & Weinman, S. T. A review on the synthesis of fully aromatic polyamide reverse osmosis membranes. *Desalination* **502**, 114939 (2021).
3. Mulhearn, W. D. & Stafford, C. M. Highly permeable reverse osmosis membranes via molecular layer-by-layer deposition of trimesoyl chloride and 3,5-diaminobenzoic acid. *ACS Appl. Polym. Mater.* **3**, 116–121 (2021).
4. Waheed, A. et al. Synthesis of co-polyamide reverse osmosis membrane constituting a linear aliphatic triamine and m-phenylenediamine for enhanced desalination performance. *Desalination* **549**, 11631 (2023).
5. Cheng, X. et al. Finely tailored pore structure of polyamide nanofiltration membranes for highly-efficient application in water treatment. *Chem. Eng. J.* **417**, 127976 (2021).
6. Aljubran, M. A. et al. Highly efficient size-sieving-based removal of arsenic(III) via defect-free interfacially-polymerized polyamide thin-film composite membranes. *J. Memb. Sci.* **652**, 120477 (2022).
7. Yuan, B. et al. Semi-aromatic polyamide nanofiltration membranes with tuned surface charge and pore size distribution designed for the efficient removal of Ca^{2+} and Mg^{2+}. *Sep. Purif. Technol.* **220**, 162–175 (2019).
8. Morgan, P. W. Interfacial polymerization. *Encycl. Polym. Sci. Technol.* https://doi.org/10.1002/0471440264.pst168 (2011).
9. Song, Y., Fan, J. B. & Wang, S. Recent progress in interfacial polymerization. *Mater. Chem. Front.* **1**, 1028–1040 (2017).
10. Wang, Z. et al. Manipulating interfacial polymerization for polymeric nanofilms of composite separation membranes. *Progr. Polym. Sci.* **122**, 101450 (2021).
11. Wang, R. et al. Thin-film composite polyamide membrane modified by embedding functionalized boron nitride nanosheets for reverse osmosis. *J. Memb. Sci.* **611**, 118382 (2020).
12. Park, H. M., Jee, K. Y. & Lee, Y. T. Preparation and characterization of a thin-film composite reverse osmosis membrane using a polysulfone membrane including metal-organic frameworks. *J. Memb. Sci.* **541**, 510–518 (2017).
13. Yan, F. et al. Improving the water permeability and antifouling property of thin-film composite polyamide nanofiltration membrane by modifying the active layer with triethanolamine. *J. Memb. Sci.* **513**, 108–116 (2016).
14. Saenz De Jubera, A. M., Gao, Y., Moore, J. S., Cahill, D. G. & Mariñas, B. J. Enhancing the performance of nanofiltration membranes by modifying the active layer with aramide dendrimers. *Environ. Sci. Technol.* **46**, 9592–9599 (2012).
15. Yong, Z., Sanchuan, Y., Meihong, L. & Congjie, G. Polyamide thin film composite membrane prepared from m-phenylenediamine and m-phenylenediamine-5-sulfonic acid. *J. Memb. Sci.* **270**, 162–168 (2006).
16. Perera, D. H. N., Song, Q., Qiblawey, H. & Sivaniah, E. Regulating the aqueous phase monomer balance for flux improvement in polyamide thin film composite membranes. *J. Memb. Sci.* **487**, 74–82 (2015).
17. Chen, D. et al. Influence of l-arginine on performances of polyamide thin-film composite reverse osmosis membranes. *RSC Adv.* **9**, 20149–20160 (2019).
18. Xu, R. et al. Influence of l-lysine on the permeation and antifouling performance of polyamide thin film composite reverse osmosis membranes. *RSC Adv.* **8**, 25236–25247 (2018).
19. Gabelich, C. J., Frankin, J. C., Gerringer, F. W., Ishida, K. P. & Suffet, I. H. Enhanced oxidation of polyamide membranes using monochloramine and ferrous iron. *J. Memb. Sci.* **258**, 64–70 (2005).
20. Ahmad, T., Guria, C. & Mandal, A. Enhanced performance of salt-induced Pluronic F127 and bentonite blended polyvinyl chloride ultrafiltration membrane for the processing of oilfield produced water. *J. Water Process Eng.* **34**, 101144 (2020).
21. Chen, D. et al. Enhancing the permeability and antifouling properties of polyamide composite reverse osmosis membrane by surface modification with Zwitterionic Amino Acid l-Arginine. *Adv. Mater. Interfaces* **6**, 1900706 (2019).
22. Waheed, A., Baig, U. & Aljundi, I. H. Fabrication of polyamide thin film composite membranes using aliphatic tetra-amines and terephthaloyl chloride crosslinker for organic solvent nanofiltration. *Sci. Rep.* **13**, 11691 (2023).
23. Lu, D. et al. Separation mechanism, selectivity enhancement strategies and advanced materials for mono-/multivalent ion-selective nanofiltration membrane. *Adv. Membr.* **2**, 100032 (2022).
24. Wang, L. et al. Salt and water transport in reverse osmosis membranes: beyond the solution-diffusion model. *Environ. Sci. Technol.* **55**, 16665–16675 (2021).

25. Yang, H. et al. Covalent organic framework membranes through a mixed-dimensional assembly for molecular separations. *Nat. Commun.* **10**, 2101 (2019).
26. Tansel, B. et al. Significance of hydrated radius and hydration shells on ionic permeability during nanofiltration in dead end and cross flow modes. *Sep. Purif. Technol.* **51**, 40–47 (2006).
27. Bartels, C., Franks, R., Rybar, S., Schierach, M. & Wilf, M. The effect of feed ionic strength on salt passage through reverse osmosis membranes. *Desalination* **184**, 185–195 (2005).
28. Ahmad, T., Waheed, A., Abdel-Azeim, S., Khan, S. & Ullah, N. Three new turn-on fluorescent sensors for the selective detection of Zn^{2+}: Synthesis, properties and DFT studies. *Arab. J. Chem.* **15**, 104002 (2022).
29. Karmakar, A. et al. Tertiary-butoxycarbonyl (Boc) – A strategic group for N-protection/deprotection in the synthesis of various natural/unnatural N-unprotected aminoacid cyanomethyl esters. *Tetrahedron Lett.* **59**, 4267–4271 (2018).
30. Li, Y. et al. Facile polyamide microstructure adjustment of the composite reverse osmosis membrane assisted by PF127/SDS mixed micelles for improving seawater desalination performance. *Desalination* **521**, 115395 (2022).
31. Ma, L. et al. Enhancing antifouling property of reverse osmosis membranes via surface tethered with the aminated cation of ionic liquids. *Desalination* **517**, 115257 (2021).
32. Choi, W., Choi, J., Bang, J. & Lee, J. H. Layer-by-layer assembly of graphene oxide nanosheets on polyamide membranes for durable reverse-osmosis applications. *ACS Appl. Mater. Interfaces* **5**, 12510–12519 (2013).
33. Shao, F. et al. Layer-by-layer self-assembly TiO_2 and graphene oxide on polyamide reverse osmosis membranes with improved membrane durability. *Desalination* **423**, 21–29 (2017).
34. Lin, S., Huang, H., Zeng, Y., Zhang, L. & Hou, L. Facile surface modification by aldehydes to enhance chlorine resistance of polyamide thin film composite membranes. *J. Memb. Sci.* **518**, 40–49 (2016).
35. Song, X. et al. Intrinsic nanoscale structure of thin film composite polyamide membranes: connectivity, defects, and structure-property correlation. *Environ. Sci. Technol.* **54**, 3559–3569 (2020).
36. Dalvi, V., Tang, Y. P., Chung, T. S., Dalvi, V. & Staudt, C. Influential effects of nanoparticles, solvent and surfactant treatments on thin film nanocomposite (TFN) membranes for seawater desalination. *Desalination* **420**, 216–225 (2017).
37. Zhao, Q., Zhao, D. L. & Chung, T. S. Nanoclays-incorporated thin-film nanocomposite membranes for reverse osmosis desalination. *Adv. Mater. Interfaces* **7**, 1902108 (2020).

Acknowledgements

The authors gratefully acknowledge the support provided by the Deanship of Research Oversight and Coordination (DROC) and also the Interdisciplinary Research Center for Membranes and Water Security (IRCMWS), King Fahd University of Petroleum and Minerals (KFUPM). The authors; Abdul Waheed, Fahad Ayesh Alharthi, Christopher Michael Fellows, Umair Baig and Isam H. Aljundi also acknowledge the Water Technologies Innovation Institute & Research Advancement (WTIIRA), Saudi Water Authority (SWA) through project # CMWS2590.

Author contributions

Hilal Ahmad: writing – review & editing, visualization, validation, resources, project administration, investigation, funding acquisition, formal analysis. Abdul Waheed: conceptualization, writing – review & editing, visualization, validation, resources, project administration, investigation, funding acquisition, formal analysis. Fahad Ayesh Alharthi: writing – review & editing, visualization, validation, resources, investigation, formal analysis. Christopher Michael Fellows: writing – review & editing, visualization, validation, resources, investigation, formal analysis. umair baig: writing – review & editing, visualization, validation, resources, investigation, funding acquisition, formal analysis. Isam H. Aljundi: conceptualization, writing – review & editing, visualization, validation, resources, project administration, investigation, funding acquisition, formal analysis.

Competing interests

The authors declare no competing interests.

Additional information

Correspondence and requests for materials should be addressed to Abdul Waheed or Isam H. Aljundi.

Reprints and permissions information is available at http://www.nature.com/reprints

Publisher's note Springer Nature remains neutral with regard to jurisdictional claims in published maps and institutional affiliations.